International Journal of Information Sciences and Engineering | *ISSN 1694-4496*
Published by AIR JOURNALS | *https://airjournal.org/ijise*
16/18 Avenue des Longaniers, Quatre Bornes, Mauritius
airjournals@gmail.com; enquiry@airjournal.org

SCHOLARLY ARTICLE

Extruded Al-Fe-Si-V Melt-Spun Ribbons for High-Temperature Applications: Process Optimization and Characterization

Nnamchi, Paul[1,2] and Obayi, C. O.[3]

[1]Department of Metallurgical Materials Engineering, University of Nigeria, Nsukka
[2]Faculty of Mechanical, Maritime and Materials Engineering (3mE), Delft University of Technology, Netherlands
[3]RSP Technology, Metaalpark 2 9936 BV Delfzijl, The Netherlands

Accepted: July 15th, 2018	Published: July 31st, 2018

Citations - APA

Nnamchi, P. and Obayi, C. O. (2018). Extruded Al-Fe-Si-V Melt-Spun Ribbons for High-Temperature Applications: Process Optimization and Characterization. *International Journal of Information Sciences and Engineering, 2(1), 1-13.*

ABSTRACT

Although the extrusion conditions of A8009 aluminium alloys play a significant role in enhancing their mechanical and dynamic properties, the impact of extrusion degrees on the increased temperature reliability of this high temperature A8009 aluminium alloy has not been studied. Here, we compare the mechanical properties of Al-8.77Fe-1.27V-0.31Si alloys at varying degrees of extrusion and find that, at high temperatures, these parameters follow the opposite pattern. With a better grasp of the connection between extrusion conditions and high-temperature dependability thanks to this research, the alloy can be further refined for use in a variety of crucial automotive and aerospace components through the adoption of stricter manufacturing standards.

Keywords: *Process Optimization; Al-Fe-Si-V Melt-Spun Ribbons; High-Temperature Applications*

Background

Among the several aluminium alloy concepts, Al-Fe systems with hypereutectic compositions and low ternary and quaternary additions, such as Si, Mn, W, V, and Cr among others are attractive candidates (Shaobo, Lijing, Hui, Hu, 2016). However, a significant disadvantage of the alloy is the insoluble nature of the essential transition elements and some rare earth metals in the aluminium matrix (Nnamchi, Leeflang, Zhou, & Bosch, 2008). Recently, notable progress has been made in this area by Nnamchi, at al (2008), who has produced high strength, melt spun Al- (V, Cr, Mn)-Fe, Co, Ni) with good ductility's. In the last few decades, a combination of melt spinning and extrusion has been used to produce fine-grained 7000 and 8000 Al alloy series (Han, Chen, Zhang, & Xia, 2016), such as AlMgAg alloy (Emrah et al, 2015), AlFeSiVMn alloy (Yang, Hsu & Chang, 1997), AlCrFeSi alloy (Conter, 1994), AlFeV alloy (Boswell & Chadwick, 1977) AlFeVSi alloy, and AlFeSi alloy (Fredrickson, Ostlund & Soderhjelm, 1984). Of all-these, Al-Fe-Si-V alloy system exhibited the best remarkable tensile strength combined with good ductility at room temperature, because Si and V can either operate as grain refiners (Shi et al, 1997, Zener & Hollomon, 1944). The microstructures have been described as nanoscale quasicrystalline or amorphous particles depending on the processing conditions (Ashrafi, Enayati, & Emad, 2014; Yaneva, Petrov, Petrov, Stoichev, & Kuziak, 2009). However, despite great success in developing this alloy, the automotive and aerospace application/market still demands further improved performance, particularly with regard to elevated temperature strength to be comparable to titanium alloys.

Compared to traditional solidification methods, prior research has shown that rapid solidification techniques produce microstructures with finer grain sizes, increased alloying element solubility, decreased segregation levels and, in some cases, the formation of metastable crystalline and amorphous phases (Shaobo, Lijing, Hui, Hu, 2016; Ashrafi, Enayati, Emad, 2014). Alloy systems benefit from these effects by having better mechanical, magnetic, electrical, and other properties. Due to these improved properties, rapid solidification processing is progressively being used in a variety of applications (Shaobo et al, 2016; Ashrafi, Enayati, Emad, 2014) to produce materials. This technology has been used in numerous automotive and aerospace components where high strength to weight ratios are sought since the creation of the melt spinning technique by Mr. Pol Duwez at Caltech and extensive study in Allied Signal (Shaobo, 2016). Its rapid cooling rate of up to 10^5—10^7 K/s aids microstructure refinement, segregation reduction, and solid solubility enhancement (Boswell, Chadwick, 1997). For this, melt spinning is described as the most cost-effective of all the rapid solidification methods, such as gas atomization and spray forming (Fredrickson, Ostlund, & Soderhjelm, 1984).

Previous studies (Yaneva, Petrov, Stoichev, & Kuziak, 2009; Yang, Hsu, & Chang, 1997) have found a connection between processing parameters and Al-Fe-Si-V alloy microstructure and mechanical properties. The literature, on the other hand, is inconsistent when it comes to the effect of processing parameters on high temperature mechanical properties. For example, melt spun Al-27Zn-1.5Mg-1.2Cu–0.08 Zr (average grain size 3.4m–2.3m) had a 30% improvement in strength after extrusion at 300°C, according to one study. Supersaturated melt spun Al-Sc-Zr alloys extruded at 430°C also showed a similar pattern. However, when extruded at 400°C, melt-spun 7000 series Al (grain size 2um) produced via accumulative roll bonding was significantly weaker (Ashrafi et al, 2014). Previously published computational studies (Das & Davis, 1988; Cantor, 1994) demonstrated that artificially induced non-equilibrium grain boundaries and a relatively small grain size, which is close to the region with an inverse Hall-Petch relationship (Han, Chen, Zhang, & Xia, 2006) can exacerbate the situation by introducing additional factors such as grain boundary sliding and grain rotation. These inconsistencies imply a dearth of thorough understanding of the inherent impacts of processing factors on the elevated temperature properties of aluminium materials, particularly the less investigated melt-spun aluminium materials. Earlier studies on the effect of process parameters on melt-spun Al alloys omitted considerations of thermomechanical parameters and fracture (Emrah, Murat, Seda, & Ali, 2015). To better understand the mechanisms responsible for the elevated temperature mechanical property of melt spun Al-Fe-Si-V material, we conducted a physically-based constitutive modelling study. The main objectives of this study are to investigate effects of process parameters on elevated temperature reliability of the melt spun aluminium materials.
However, a correlation of the microhardness of the ribbons to the yield strength was still higher in comparison to the usual conventional cast aluminum alloy.

Experimental Procedures

An as-spun Al-Fe-V-Si melt-spun ribbon with nominal composition 8.77% Fe, 1.27%V, 0.31%Si and balanced Al, was prepared by using industrial grade (99.7 wt%) Al, Fe, V, Si and Al-Fe master alloy at Rapid solidification Technology, Delftzijn, The Netherlands. These raw materials were melted at 720 °C and held for 30 min in an electrical resistance furnace, and finally sprayed on a rotating water-cooled copper cylinder to obtain ribbons, which has a size of 0.04mm in thickness and 1.6 mm in width was initially in an amorphous state. The phase transformation characteristics of the ribbon were determined by using a modulated differential scanning calorimeter (MDSC) of TA Instrument. Sample weights were about 5-6 mg, while the heating and cooling rates were 10°C/min. Rod-shaped billets, with dimension of 50mmin diameter and 30mm in length, were produced by filling the flakes into an aluminium mould and conventional isostatic cold pressing under 200 MPa for 8 min at room temperature. In order to decrease friction between the aluminium container and the die, zincstearic acid was employed as a lubricant throughout this procedure. Fig. 1 illustrates this. Preheating at 150 °C for a period of time ranging from 0 to 300 minutes was then applied to the billets prior to extrusion. Finally, the rod-shaped billets were extruded into 13mm rods with an extrusion ratio of 10:1 at five (Thuishield, 1974) different temperatures: 27°C, 370°C, 400°C, 430°C and 460°C, before air cooling to room temperature. To alter the strength and plasticity of melt-spun metallic materials after severe plastic deformation (SPD), subsequent annealing/recovery treatment is applied (Jacobs, 1994; Yang, Hsu, & Chang, 1997). Effect of Annealing Treatment on Mechanical Properties of Nanocrystalline a-iron: an Atomistic Study]. Several annealing treatments were performed on the billets, including 450°C for 30 min, 500°C for 15 min, 500°C for 60 min, and 60°C for 15 min in a furnace.

The samples for cross-sectional and longitudinal-sectional microstructural observations were cut perpendicular to and parallel to the extrusion direction while the microscopic observations were performed after electropolishing using a Neophot 2" optical microscope. The phase structures were examined by a Bruker Advance D8 X-ray diffraction (XRD) operating with Cu Ka radiation at 50 kV and 150 mA. The scan ranged from 20 to 100 with a step size of 0.02and a dwelling time of 0.5 s. Mechanical tests were performed on a microforce testing system from Instron at a strain rate of 3.3×10^{-4} sec^{-1} using cylindrical specimens machined from the as-extruded billets following ASTM-E8. The microforce testing system incorporates a temperature chamber linked to a microprocessor, allowing samples to be monitored while being tested at room temperature (RT), 200°C, 300°C, and 350°C till fracture, after 100 hours of annealing at 100°C, 200°C, 300°C, and 350°C. The gauge length of the samples was between 6- and 10-mm. Special attention has been paid to the accuracy and repeatability of the results. By using a rigid reference material to calibrate the strain contributed by the testing system, it is found that the error of the measured strain values is negligible within the tested range. The micro-hardness of the extruded sample was tested with a load of 100 g respectively, with a dwelling time of 10 s. The average hardness value was calculated from 7 measurements for each sample.

Results and Discussion

Evolution of Extrusion Characteristics

Figure 1(a) depicts the representative variation of extrusion pressure with ram displacement as exhibited by the melt spun ribbons deformed at various extrusion temperatures (i.e.,370°C, 400°C,430°C and 460°C) using a 10:1 reduction ratio. A comparison of the part of the pressure/ram displacement curves before the peak value (Fig.1 demonstrated an increase in force as temperature decreased, showing that material extruded at a lower temperature work hardened more quickly. Given that more severe deformation occurs at lower extrusion temperatures (between 370°C and 400°C), the presence of a higher volume fraction of dispersoids particles is almost expected to form more effective barriers by inducing grain boundary pinning at all stages of dislocation motion. Thus, limiting plastic flow and contributing to high work hardening rate (Fredrickson, Ostlund, & Soderhjelm, 1984). As illustrated in Fig. 1a, the peak value is flatter at elevated temperatures (between 430°C and 460°C) is in line with the common belief that a material's work hardening rate decreases as the temperature rises. At higher temperatures, dislocation annihilation within sub-grain interiors via cross slip and climb becomes easier. An analysis of the extrusion behaviors of the present alloy and 1XXX, 3XXX, 5XXX and 8XXX series aluminum alloy in Ref. (Boswell & Chadwick, 1977) revealed an increased pressure requirement for the present alloy. The increased resistance to deformation is related to the incorporation of high intermetallic particles into the microstructure as a result of melt spinning. The fundamental principle behind the ability of fine inclusions within the metal matrix to inhibit deformation and prevent grain growth has been established already. Given that pressure reduces considerably at elevated temperatures (and vice versa at low temperatures, it is worthwhile to investigate the relationship between temperature and material work hardening.

The correlation between the extrusion peak pressure and the reciprocal of the absolute temperature in Figure 1b is of practical importance to this study, because the peak pressure is a breakthrough value in determining whether the execution of an extrusion cycle is possible (Boswell and Chadwick, 1977). Although, the linearity in slope indicated that as temperatures increased, the peak pressure decreased progressively. The appearance of a kink (non-uniformity) at 400°C indicated the end of the correlation and indicated that the melt-spun material had a small extrusion temperature window between 370°C and 400°C. Hence, extrusion at temperatures above 400°C would likely lower the overall strength of the materials by reducing dislocation density. Several possible mechanisms are proposed to explain this phenomenon. During high temperature extrusion, the dislocation density decreases due to annihilation of dislocations with opposite Burger's vectors (Cantor, 1994). Effect of Annealing Treatment on Mechanical Properties of Nanocrystalline a-iron: An Atomistic Study] and dislocation absorption at grain boundaries.

Microstructure Analyses

Fig. 2(a) shows typical XRD patterns of the experimental samples extruded at the minimum (370°C) and highest extrusion temperatures (460°C). The melt spun sample are mainly composed of α-Al phase $Al_{11}V$, $FeAl_2$, AlFe phases and β-intermetallic phase are evident structure. Furthermore, a very weak diffraction peak from Si phase is observed, indicating its low concentration, but the intensity of diffraction peaks from both $Al_{11}V$, $FeAl_2$ phase and Si phase are notably increased compared with the highest extrusion temperatures (460°C) sample. This indicates that the precipitates of Si and $Al_{11}V$, $FeAl_2$ phases are further formed during the extrusion process. The lattice parameters of α -Al in the 370°C and 460°C extruded samples are 0.4039 nm and 0.4041 nm respectively, slightly lower than that of pure Al (0.4050 nm), which is mainly due to the Si solution into α -Al lattice. Since Si has a smaller atomic radius compared with Al, and the lattice parameter of α -Al supersaturated solid solution will decrease with the Si-concentration increase (Boswell & Chadwick, 1977). Furthermore, the existence of metastable β-intermetallic phase in the matrix indicates a high degree of refinement due to the first melt spinning experiment's high cooling speeds (10^7C/s). It is worth noting that $Al_{13}(Fe, V)_3Si$ intermetallic phases with similar lattice characteristics (a= b = 0.612 nm, c = 4.15 nm, and β=91°) have previously been linked with remarkable microstructural resistance that hinders grain coarsening (Shaobo, Lijing, Hui, & Zhang, 2016).

The deformation microstructures at different extrusion temperatures are shown in Fig. 2. The average values of the grain, sub-grain size, sub-grain and aspect ratio in specimens extruded at various temperatures are listed in Table 1. As expected, the average grain size progressively increased with extrusion temperature, according to the POM analysis. Typical example is given in Fig. 2(d). As the temperature increases to 430°C, significant change in microstructure results. The sub-grains show polyhedral shape with smaller aspect ratio, 1.6. The sub-grain size increases gradually from 0.65 to 0.9µm as the temperature increases from 370°C to 430°C, but it increases significantly to 2.2µm at 460°C The results obtained in the present investigation demonstrate that polarized optical microscopy (POM) is a convenient technique to reveal grain and sub-grain structures in the class A8000 series materials.

The microstructure was observed on sections taken in directions parallel and perpendicular to the extrusion direction Z. Due to prior billets compression with high pressure during the original production process, all the microstructure reveals characteristic melt spun ribbons with a semi-circular morphology. These results are related to deformation conditions. At very low stresses (very high temperatures extrusion - 430°C, and 460°C or/and very low strain rates), the sub-grains are very large, which makes observing the sub-grains easily in POM, (Fig.2 (a). The data of AA5052 aluminium alloy (Yang, Hsu, Chang, 1997) are compared with the present result of AA8009 aluminium. In Fig. 3, both alloys show similar increasing trend of sub-grain size with increasing extrusion temperature, but the sub-grain size of AA8009 aluminium is larger than that of alloy AA5052. The transformation of low angle borders into high angle boundaries, according to Yamashita et al. (2000) is due to the absorption of moving dislocations into the boundaries during deformation. At higher temperatures, dislocation annihilation by cross slip and climb becomes easier, giving dislocations a greater chance to be annihilated within sub-grain interiors. As a result, dislocation absorption into a boundary becomes less frequent, making the increase of boundary misorietation less efficient. The preceding demonstrates that extrusion temperature has a significant impact on both the hardening and softening processes, which is consistent with previous research (Mandal et al., 2009).

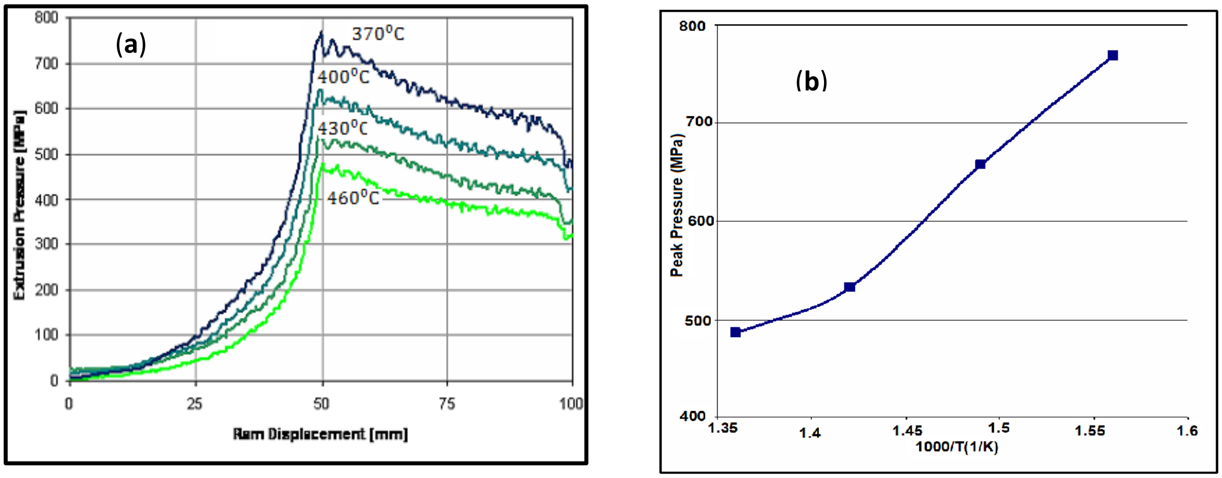

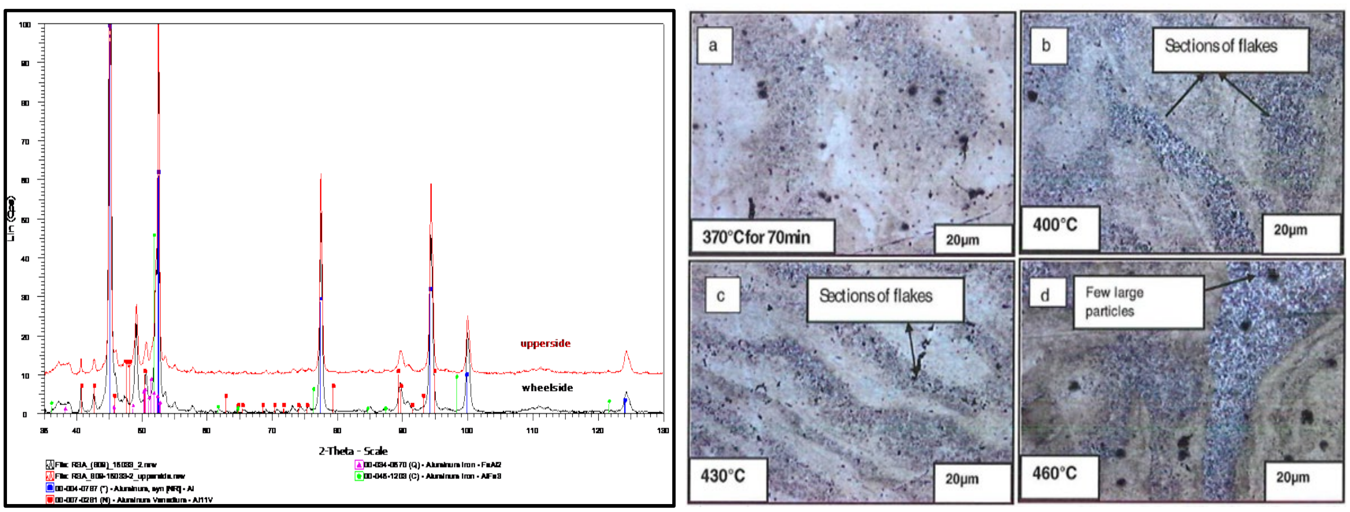

Figure 1:(a) XRD profile of material extruded at 370°C and 460°C temperatures, (b) microstructures of the material extruded at 370°C, 400°C, 430°C and 460 °C.

Precipitation Strength Contribution Predictions

A significant number of micrometre-size precipitates nucleating during extrusion were assumed to be responsible for the alloy's improved strength. The higher pressure increases in the extruded rod likely resulted from a combination of larger precipitate volume fraction and Hall-Petch strengthening. Precipitate strengthening can occur by precipitate shearing, precipitate bypass with dislocation looping, or a combination of these two processes, depending on the size and structure of the precipitate. Precipitate shearing is applicable to alloys having coherent and tiny precipitates, such as those seen in extruded melt spun Al-Fe-Si-V alloys. The Zener drag contributions were determined using quantitative XRD and electrical resistivity techniques, allowing the volume fraction and particle size to be estimated (Thuishield et al, 1974, Nnamchi, Obayi, Zhuo, & Okorie, 2009) as a function of extrusion temperatures, according to Equation (1).

$$Z_P = N_{interact} F_{MAX} = \frac{3\gamma_{GbF_V}}{2r} \qquad (1)$$

Here, Fmax ~γπr, the grain boundary energy, γ for aluminium is 0.2899 to 0.3 J/m2, and the average size and volume percentage of the dispersoids are r andF_v, respectively. Figure 3(a) compares the actual and predicted Zener drag pressure against extrusion temperatures. The current research evince the apparent Zener drag pressure (Zp) and the extrusion temperature have an inverse relationship. The agreement between calculated and measured strength change proves that Hall-Petch strengthening account for the high extrusion pressure increase (Table 3). Compared to the measured strength increase, the Hall-Petch strengthening took up ~10% of that, the majority of strengthening increase in melt-spun extruded rod was attributed to precipitation strengthening. The calculated Hall-Petch strengthening increase in extruded rod was excluded in precipitation strengthening calculation.

This is because despersoids appear to obstruct dislocation movement at grain boundaries, which is produced by particles applying a retarding force or pressure on moving grain borders during plastic flow, producing work hardening.

This effect reduces the mobility of the boundary, depending on grain boundary velocity. Therefore, during extruding between temperatures of 370°C to 400°C, a combination of high angle grain boundary energy keeps the despersoids entangled in the grain boundaries; and further reductions in particle size can even occur simultaneously, leading to high volume fractions of fine particle and eventual higher Zener drag pinning. The average particle size after extrusion at 370°C ranges between 0.1 and 1.15m, but increases with extrusion temperature. Emrah, et'al, (2015) discovered that the size dependency of silicon crystals on extrusion temperature produced the crystal size variation. Extrusion. In either case, this is sure to affect the elevated temperature reliability of the alloy. On the other hand, the result of the Zp exhibited by the samples extruded at high temperatures (i.e., 430^{0}C and 460^{0}C) have less (Z_P), and are seemingly less affected by the despersoids encountered during dislocation migration. Additionally, their smaller grain boundary energy will lead to less(Z_P), since it is directly proportional to the grain boundary energy (γ_{Gb}), according to Eqn. (1). It is perhaps also possible that some of the despersoids may have already been detached from their 'anchored' grain boundaries.

The thermal examination of materials extruded at 370°C and 460°C (Figs.1c and 1d), respectively was investigated using differential scanning calorimeter (DSC). The high temperature peaks in the DSC profile (Fig. 1c) indicate that a larger percentage of the alloy elements precipitated more readily from the aluminium matrix upon extrusion at 370°C, resulting in more closely spaced dispersoids that act as internal barriers to metal flow, hence boosting work hardening at lower temperatures. When extruded at elevated temperatures, such as 460°C (Fig.1d), a greater proportion of equilibrium solutes dissolves in the matrix, reducing dislocation emission sources and improves material ductility. Therefore, the large volume fraction of solute components and/or dispersoids in the extruded material is believed to contribute significantly to the high extrusion pressure.

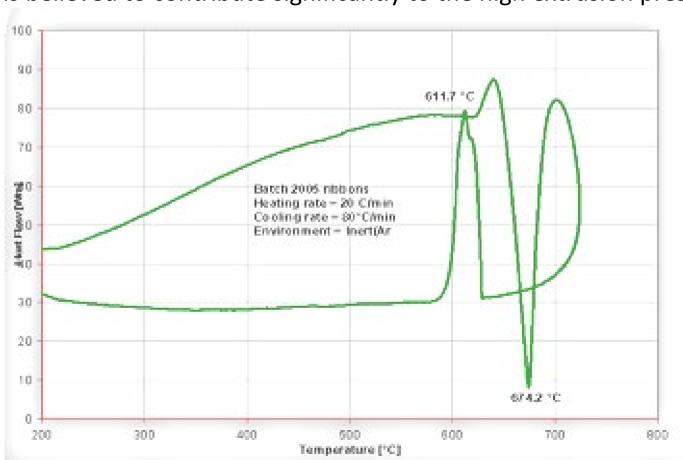

Fig: 2 True stress-strain curve and flow behaviour of A8009 aluminium alloy

The true stress-strain curves of melt spun Al-Fe-Si-V alloy obtained after extruding at different temperatures and strain rates are shown in Fig. 4. Most of the curves exhibit typical DRX behaviour with a single peak stress followed by a gradual fall toward a steady-state stress. However, the peak stress becomes less obvious when the strain rate is increased or the deformation temperature is decreased. The stress-strain curves also show that the flow stress decreases as the deformation temperature increases or the strain rate decreases. The drop in flow stress with deformation temperature may be attributed to the increase in the rate of restoration processes and the decreases in the strain hardening rate. Additionally, the temperature rises due to the heat liberated from the plastic deformation at higher strain rates (10 s-1) leads to the final drop of flow stress.

Fig. 4 illustrates the unprocessed true stress-strain curves of A8009 aluminium material obtained at various temperatures (ambient, 200,300 and 350°C) following extrusion at 370°C, 400°C, 430°C, and 460°C. Only three data were provided since the materials extruded at 460°C failed prematurely during the test and could not resist additional deformation. As can be seen, most of the curves exhibit typical DRX behaviour with a single peak stress followed by a gradual fall toward a steady-state stress. However, the peak stress becomes less obvious when the strain rate is increased or the deformation temperature is decreased. The stress-strain curves also show that the flow stress decreases as the deformation temperature increases or the strain rate decreases. The drop in flow stress with deformation temperature may be attributed to the increase in the rate of restoration processes and the decreases in the strain hardening rate. Additionally, the temperature rises due to the heat liberated from the plastic deformation at higher strain rates (10 s-1) leads to the final drop of flow stress.
A series of in situ tensile tests were carried out at four temperatures, namely, 20°C, 200^{0}C, 300^{0}C and 350^{0}C, respectively on the as extruded samples to investigate the effect of extrusion treatment on mechanical performance of the A8009 aluminium alloy. The extrusion temperatures are 370^{0}C, 400^{0}C, and 430^{0}C, respectively. The samples extruded at 460^{o}C did not withstand any further deformation as they fractured prematurely during the test. The unprocessed tensile stress-strain curves of the as-extruded A8009 aluminium alloy for the respective temperature conditions is shown in Figs. 4. In spite of the differences in the shape of the curves and specific flow stress value with respect to temperature, all the flow stress curves demonstrate three characteristics of the flow stress curves that occur during deformation: (a) an initial rapid increase in the stress to a peak value (i.e. the first work-hardening regime), (b) the stage at which stress peak is attained and (c) the flow stress decreases monotonically towards a steady state regime with a varying softening rate which typically indicates the onset of DRX.

Comparing the curves shown in Fig. 4 with each other and together with the data in Table 2, reflect the flow curves is sensitively dependent on both extrusion and deformation temperature. The observed initial work hardening is clearly due to dislocation generation and accumulation caused by plastic deformation (Boswell, Chadwick, 1977). This is because, dislocation movement is impeded at grain boundaries and intermetallic particles, which restricts the plastic flow and contributes to work hardening (Fredrickson et al, 1984). Although, after a rapid increase in the stress to a peak value, in all the curves the flow stress decreases monotonically towards a steady state regime with a varying softening rate which typically indicates the onset of DRX, (See Fig. 4 and Table 2). As onset of DRV relies heavily on the critical activation energy and dislocation density. Implicitly, indicating that strain-softening effect might be the more dominant factor than the work-hardening effect. On another hand, since the overall flow stress shows a marked decline with increasing temperature, due to a reduced critical shear stress and an improvement in the mobility of grain boundaries. In this case, it is possible that the strain-softening effect is weakened with high deformation temperatures as dislocation annihilations increase. This is because higher temperature deformation provides longer time for the energy accumulation and higher mobilities at grain boundaries, which result in the nucleation and growth of dynamically recrystallized grains and dislocation annihilation. For the A8009 alloy studied, the peak stress occurs over a strain range of 0.05–0.25 where the work-hardening and strain-softening effects reach a dynamic equilibrium under most of the deformation conditions applied.

Table 1: effect of extrusion condition on plastic flow of the alloy

		Strain (%) / Strain hardening rate at different temperatures			
Extrusion Temp. (K)		**273K**	**473K**	**573K**	**623K**
1	643	12/ 0.62	13/0.59	13.7/0.5	13.8/1.24
2	673	16.5/0.57	17.1/0.51	17.3/0.51	14.1/1.36
3	703	12.6/0.6	12.4/0.59	15.9/0.54	16.3/1.17

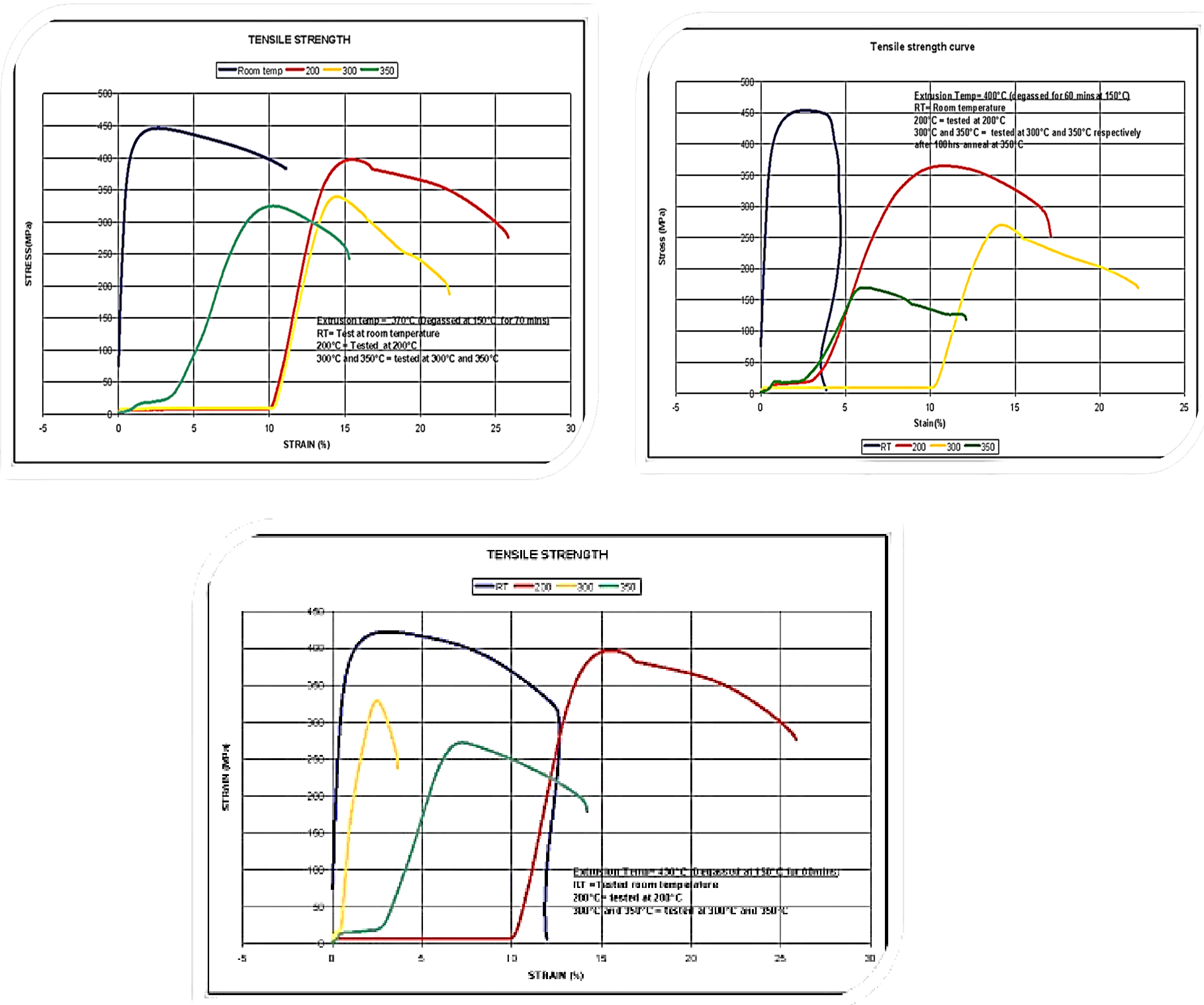
TENSILE STRENGTH
Room temp
200
300
350
STRESS(MPa)
STRAIN (%)
Extrusion temp = 370°C (Degassed at 150°C for 70 mins)
RT= Test at room temperature
200°C = Tested at 200°C
300°C and 350°C = tested at 300°C and 350°C
Tensile strength curve
Extrusion Temp= 400°C (degassed for 60 mins at 150°C)
RT= Room temperature
200°C = tested at 200°C
300°C and 350°C = tested at 300°C and 350°C respectively after 100hrs anneal at 350°C
Stress (MPa)
Stain(%)
RT
200
300
350
TENSILE STRENGTH
RT
200
300
350
STRAIN (%)

Fig.3

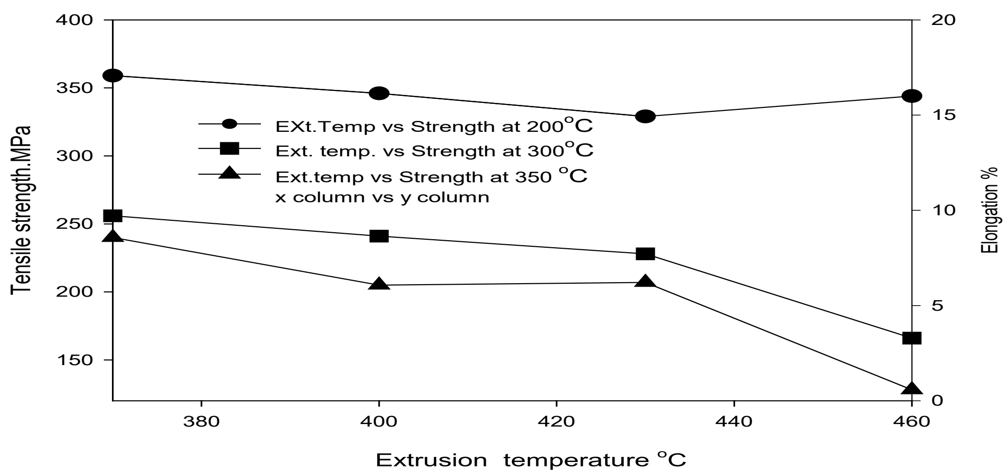
EXt.Temp vs Strength at 200°C
Ext. temp. vs Strength at 300°C
Ext.temp vs Strength at 350 °C
x column vs y column
Tensile strength.MPa
Elongation %
Extrusion temperature °C

Fig. 4

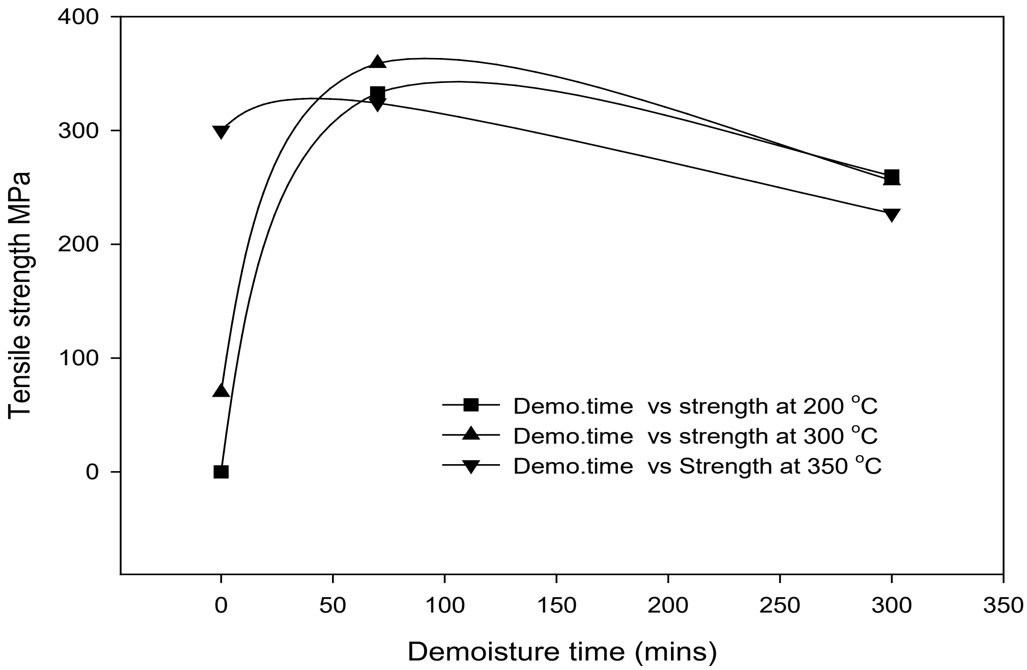

Analysis of the Constitutive Behaviour

Previously, several empirical equations have been proposed to determine the deformation activation energy and hot deformation behaviour of alloys. The most frequently used is Arrhenius equation (See eqn. 4) which describes the behaviour of the material deformed at different temperatures and strain rates. The effects of the temperatures and strain rate on the deformation behaviour can be represented by Zener-Hollomon parameter, Z in an exponent-type equation. However, it has been shown that during hot deformation, the relationship between flow stress, strain rate and temperature described by a sine hyperbolic law in the Arrhenius type equation proposed by Sellar and Tegart (Eqn.7) gives better approximations between Z parameter and stress (Thuishield et al., 1974, Nnamchi et'al, 2009, Das and Davis, 1988, Shaobo et'al, 2016).

$$Z = |\dot{\varepsilon}| exp\left(\frac{-Q}{RT}\right) \tag{4}$$

$$|\dot{\varepsilon}| = AF(\sigma) exp\left(\frac{-Q}{RT}\right), \tag{5}$$

$$\text{thus: } F(\sigma) = \begin{Bmatrix} [\sigma]^n & \alpha|\sigma| < & 0.5 \\ exp(\beta|\sigma|) & \alpha|\sigma| > & 1.4 \\ [Sinh(\alpha|\sigma|)]^n & for\ all & \sigma \end{Bmatrix} \tag{6}$$

In which, $\dot{\varepsilon}$ is the strain rate (s^{-1}), R is the universal gas constant (8.31 $J.mol^{-1}.K^{-1}$), T is the absolute temperature (K), Q is the activation energy for DRX ($kJ.mol^{-1}$), serves as an indicator of deformation difficulty degree in the plasticity deformation theory, σ is the flow stress (MPa) for a given stain, A, α , Q and n are the material constants that are dependent of deformation temperatures., $\alpha = {}^{\beta}/_{n}$. The flow stress data used in the constitutive analysis were obtained from the average value of tensile tests at strains between 0.5 and 1.4. These are listed in Table 3. The flow stress values obtained from the tensile tests at a strain rate of 3.3 x 10^{-4} sec^{-1} were corrected for adiabatic deformation heating (Cantor, 1994).

For all the stress level (including low and high stress levels), by, substituting Zener-Hollomon parameter (eqn.4) into (eqn.5), thus, the flow stress can be expressed as eqn. 7.

$$|\sigma| = \frac{1}{\alpha} In \left\{ \left({}^{Z}/_{A} \right)^{\frac{1}{n}} + \left[\left({}^{Z}/_{A} \right)^{\frac{2}{n}} + 1 \right]^{\frac{1}{2}} \right\} \qquad (7)$$

For all the stress level (including low and high stress levels), the relationships between flow stress and strain rate can be represented as the following:

$$|\dot{\varepsilon}| = A[Sinh(\alpha|\sigma|)^n]exp\left(\frac{-Q}{RT}\right) \qquad (8)$$

Taking the logarithm of both sides of Eq. (8), we arrive at:

$$In\dot{\varepsilon} = InA - \frac{Q}{RT} + n.In[sinh(\alpha\sigma)] \qquad (9)$$

By substituting the values of the flow stress and strain under different temperatures and strain rates can be identified for the present target stresses. The linear relationships between $In[sinh(\alpha\sigma)]$ and 1000/T were fitted out as Figure 6, where the mean value of the slope rates is accepted as Q/(Rn) value and Equation 7 can be rewritten as:

$$Q = R_{ns} = R_n \frac{\partial In[sinh(\alpha\sigma)]}{\partial \frac{1}{T}} \qquad (10)$$

The Polynomial fitting results of Q, n, ln A and α of A8009 aluminium alloy at various temperature is listed in Table 3. From the fitting results, the average Q value at room temperature was calculated to be 174 kJ/mol. Eq. (8) could thus be written as:

$$\dot{\varepsilon} = A[Sinh(\alpha\sigma)^n]exp\left(\frac{-174 \times 10^3}{8.314 * T}\right) \qquad (11)$$

The value of activation energy Q determined in the present study is inversely proportional to deformation temperature, but much larger than the value for the self-diffusion of pure aluminium (135 kJ/mol) and slightly larger than the activation energy values, such as as-extruded strain hardened 7075 aluminium alloy (96.1749 10 kJ/mol) [A Characterization for the Flow Behaviour of As-Extruded 7075 aluminium alloy By the Improved Arrhenius Model with Variable Parameters]. This is because of the dislocation climb mechanisms, rather than diffusion in pure metal, and because, dislocation movement is impeded at grain boundaries and intermetallic particles, which restricts the plastic flow during deformation. It is important to note that the present A8009 alloy under investigation was in the as-extruded state and as such is expected to contain strong initial as extruded texture before the tensile tests, and therefore the corresponding activation energy might be slightly larger than the value of the as-extruded and homogenized alloy. Simply put, the small difference in the activation energy for deformation is attributed to the difference in material processing history. Conclusions The high temperature deformation behaviour of 05Cr17Ni4Cu4Nb steel were investigated by hot compression test in the temperature range of 1000-1200°C, strain rate range of 0.01-10s-1 and strain range of 0-0.9. The main conclusions can be obtained as follows:

i. The flow stress of 05Cr17Ni4Cu4Nb steel during hot compressive process decreases with increasing deformation temperature and decreasing strain rate.
ii. Microstructural observation confirms the occurrence of DRX behaviour and the dynamic recrystallization grain size decreases with decreasing deformation temperature and increasing strain rate.
iii. The constitutive equation was established with material constants expressed by a fourth order polynomial fitting of strain to describe the influences of temperature, strain rate and strain on high temperature deformation behaviours of 05Cr17Ni4Cu4Nb steel.

Conclusion

The present paper focused on the microstructure and mechanical properties of Al-8.5Fe-1.3V-1.7- Si(wt%) alloy parts fabricated by electronlasermelting (EBM). The following conclusions can be obtained.

i. The comparison between the microstructures of the extruded materials after hot isostatic pressing at 425 °C) as used in this study showed that by direct extrusion temperature at 370oC and solution treatment at 200°C for 100hrs, the optimum operating temperature for this alloy should not be more than 300°C.
ii. The microstructure of this melt spun aluminium alloy is characterized by a very fine dispersoids and the coarsening during solution treatment and high temperature tensile testing were quite limited.
iii. This homogenously distributed fine grain dispersoids are responsible for the thermal stability and high mechanical strength at elevated temperature up to 350°C. Thus, coarsening of the microstructure due to exposure to high temperatures were prevented by cold compaction.

Acknowledgements

The authors gratefully acknowledge the materials and moral support by the then Materials Science and Engineering Department, TUDelft and RSP Technology, Metaalpark 2 9936 BV Delfzijl, both in The Netherlands

References

Ashrafi, H., Enayati, M. H., Emadi, R. (2014) Nanocrystalline Al/Al12(Fe, V)3Si alloy prepared by mechanical alloying: Synthesis and thermodynamic analysis. *Advanced Powder Technology,* 25, 1483-1491

Boswell, P.G. and Chadwick, G. (1977). The grain size of splat quenched alloys. *Scripta Met*., **2**, 459-465.

Cantor, B. (1994). Development of microstructure in advanced solidification processing. *Micron*, **25**, 551-556.

Das, S. K. and Davis, L. A. (1988). High-performance aerospace alloys via RS processing. *Materials Science and Engineering,* 98, 1-12

Emrah, K., Murat, B., Seda, S., Ali, K. (1997). Dry sliding wear behaviour of Al–Fe–Si–V alloys at elevated temperatures, *Wear* 322-323, 101–107

Fonstein, N. (2015). Advanced High Strength Sheet Steels: Physical Metallurgy, Design, Processing, and Properties. Springer International Publishing: New York, NY, USA, 2015.

Fredrickson, H., Ostlund, A., & Soderhjelm, H. (1984). A theoretical study of the transition from crystalline to amorphous structure in alloys produced by the Melt-spinning. *Rapid Quenching of Metals,* 3-7, 187-200.

Jacobs, M.H. et. al. (1974). The microstructure of Al-8%Fe –based alloys prepared by rapid quenching from liquid state. *J.Mat.Sci. & Eng.*, 9.

Jones, H. (1969). Observations on a structural Transition in aluminium alloys hardened by rapid solidification. *J. Mat. Sci. & Eng.,* 5, 1-18.

Nnamchi, P. S., Obayi, J. U., Zhuo, J. & Okorie, B. O. (2009). Process optimization and characteristics of casting conditions of melt-spun Al-Fe-Si ribbons for elevated temperature aerospace application. *Journal of Nigeria Metallurgical and Mater. Eng.*, 4(2), 10-18.

Nnamchi, P., Leeflang, Marius, Zhou, J. & Bosch, A. J. (2008). Characterization of Melt-Spun AA8009 Alloy and Extrusion Process Optimization. *Proceedings of the Euro International Powder Metallurgy Congress and Exhibition, 2*

Sahoo, K. L., Pathak, B. N. (2009). Solidification behaviour, microstructure and mechanical properties of high Fe-containing Al–Si–V alloys. *J. Mater. Proc. Techn.,* 209, 798-804.

Shaobo, Sun, Lijing, Zheng, Hui Peng, Hu Zhang (2016). Microstructure and mechanical properties of Al-Fe-V-Si aluminium alloy produced by electron beam melting. *Mater. Sci. & Eng. A.,* 659, 207-214

Shaobo, Sun, Lijing, Zheng, Hui, Peng, Hu, Zhang (2016). Microstructure and mechanical properties of Al-Fe-V-Si aluminium alloy produced by electron beam melting. *Materials Science & Engineering*, 659, 207–214.

Shi, H., McLaren, A. J., Sellars, C. M., Shahani, R. & Bolingbroke, R. (1997). Constitutive equation for high temperature flow stress of aluminium alloys. *Materials Science and Technology*, 13, 210-216. http://dx.doi.org/10.1179/026708397790302421

Skinner J. D. J. et al. (1986). Dispersion strengthened AI-Fe-V-Si alloys. *Scr. Met.,* 20, 867-872.

Sobolev, S. L (1997). Rapid solidification under nonequilibrium conditions. *Physical Rev. E*., 55-60.

Thuishield, G. et al. (1974). Mechanical properties of Al-8wt%Fe –based alloys prepared by rapid quenching from liquid state. *J. Mat & Eng.,* 9, 1644-1660.

Yamashita, A, Yamaguchi, D, Horita, Z., Langdon, T. G. (2000). *Mater Sci Eng*

Yaneva, S., Petrov, K., Petrov, R., Stoichev, N., Kuziak, R. (2009). Influence of silicon content on phase development in Al–Fe–V–Si alloys, *Mater.S Sci. & Eng. A*, 515, 59-65

Yang, C. C., Hsu, W. M., & Chang, E. (1997). Wear performance of Al–Fe–V–Si particle reinforced cast aluminium alloy composites. *Mater. Sci. Technol.* 13 (8), 687–694.

Yang, J., Zhang, J., Dai, Y., Ma, J., Sun, B. (2015). Ab initio simulation: The correlation between the local melt structure and segregation behaviour of Fe, V, Ti and Si in liquid Al. *Computational Materials Science*, 109, 41-48.

Zener, C. & Hollomon, H. (1944). Effect of strain-rate upon the plastic flow of steel. *Journal of Applied Physics*, 15, 22-27. http:// dx.doi.org/10.1063/1.1707363

APPENDIX I

Table 2

Extrusion Temp. **(°C)**	Demoisturing time (min)	Strain hardening rate (given by the difference between UTS and the 0.2% proof strength)			
		RT	200 ºC	300 ºC	350 ºC
370	0	59	4	-	109
370	70	62	9	5	24
370	300	54	0	16	95
400	70	57	10	10	36
430	70	60	59	14	17
460	70	63	197	6	4